Inflation and collapse of the Wai'anae volcano (Oahu, Hawaii, USA): implications from rock magnetic properties and magnetic fabric data of dikes

Emilio Herrero-Bervera, Bernard Henry, Mário Moreira

Herrero-Bervera *et al.*
Earth, Planets and Space (2018) 70:190
https://doi.org/10.1186/s40623-018-0960-z

Earth, Planets and Space

FULL PAPER Open Access

Inflation and collapse of the Wai'anae volcano (Oahu, Hawaii, USA): implications from rock magnetic properties and magnetic fabric data of dikes

Emilio Herrero-Bervera[1*], Bernard Henry[2] and Mário Moreira[3,4]

Abstract

In order to investigate the role of dikes in the volcanic evolution and the triggering mechanisms of catastrophic mass wasting volcanoes, we have sampled for a pilot study, seven dikes within the Wai'anae volcano, Oahu, Hawaii. The width of the dikes ranged between 0.4 and 2.5 m. This work focuses on the characterization of the magma flow directions using anisotropy of magnetic susceptibility (AMS) data in dikes of the inner part of the Wai'anae volcano. This part is now exposed, because this volcano experienced destabilization and flank collapse. Rock magnetism data show composite magnetic mineralogy, corresponding when plotted on the Day diagram to be dominated by single domain (SD) and pseudo-single domain particles of pure titanomagnetite, suggesting possible inverse magnetic fabric associated with the SD grains. The obtained magnetic fabric does not reflect such grain sizes and is probably partly related to the presence of different magnetic phases, resulting in part of our samples as having "abnormal" fabrics. We therefore used a simple criterion to eliminate most of the abnormal fabrics in order to analyze the magnetic fabric data in a clearer way. After rejection of most of the abnormal data, the determination of the magnetic zone axis, which underlines the effect of imbrication in dike margins, yielded reliable magma flow directions in most of the studied dikes, with a predominance of vertical to subvertical AMS directions. The inferred dominantly vertical to subvertical magma flow of dikes (feeding from below) within the most internal parts of the volcano, suggests a process of accumulation of new magma at different levels within the inner part of the edifice. This process was enhanced by subhorizontal magma flow toward the volcano center in two other dikes. Such accumulation helps to explain the inflation, subsequent destabilization, and flank collapse of the Wai'anae volcano.

Keywords: Dikes, Volcano, Hawaii, Magnetic fabric, Flow direction

Introduction

Dike swarms are present in all basaltic volcanic systems, but in only a few cases erosion allows us to view them directly. Much of what is known about those swarms, comes from the monitoring of ground deformation and seismicity in active rift zones. Accordingly, many basic questions about the emplacement of these intrusions have not been resolved, like the intrusion geometry and distribution of dikes swarms, the variations in the dike population and the swarm intensities at varying distances from the volcanic focus. How magma is partitioned between dikes and sills is still unclear. Our long-term general objective is to make a comparative study of the dike characteristics, from quantitative field measurements, anisotropy of magnetic susceptibility (AMS) and rock magnetism data of the intrusive complexes in Hawaii. Today we know that, during the development of Hawaiian volcanoes, a relative rapid growth occurs as well as a volcanic flank collapse of the central volcano due to endogenic and exogenic processes (Voight

*Correspondence: herrero@soest.hawaii.edu
[1] Petrofabrics and Paleomagnetics Laboratory, SOEST-Hawaii Institute of Geophysics and Planetology, University of Hawaii at Manoa, 1680 East-West Road, POST 602, Honolulu, HI 96822, USA
Full list of author information is available at the end of the article

and Elsworth 1997; Keating and McGuire 2000; Reid et al. 2001; Rubin and Pollard 1988; Elsworth and Day 1999; Silva et al. 2012, 2018). These large mass wasting phenomena have been identified and studied in great detail on a global scale (e.g., Lipman et al. 1988; Moore et al. 1989; Presley et al. 1998; Day et al. 1999; Moore and Clague 2002; Yokose 2002; Coombs et al. 2004; Hildenbrand et al. 2006; Battaglia et al. 2011; Costa et al. 2015).

In the last three decades, it has been clearly demonstrated that paleomagnetism and rock magnetism of magmatic rocks have mainly advanced the knowledge in geophysics, geology and volcanology. They provide a correlation or indirect dating tool to document the tilting and rotation of the rocks, and a way of assessing the thermal history of rocks. Flow direction in dikes is difficult to determine, particularly in fine-grained rocks such as basalts. Those determinations are generally based on the analysis of the preferred orientation of the contained minerals. Various approaches, based on texture analysis (Leiss et al. 2000), have been attempted for basaltic lava flows, but the interpretation remains difficult and disputable because of the nearly isotropic distribution of small grains in volcanic rocks. This is why the AMS technique is now frequently used to study the flow of lavas and dikes in general (e.g., Hargraves et al. 1991; Ellwood 1978; Fanjat et al. 2012; Féménias et al. 2004; Staudigel et al. 1992; Raposo 1997, 2011; Raposo and Ernesto 1995; Moreira et al. 1999, 2014; Rochette et al. 1999; Aifa et al. 1999; Callot et al. 2001; Herrero-Bervera et al. 2001, 2002a, b; Archanjo et al. 2002; Callot and Geoffroy 2004; Cañón-Tapia 1996, 2004; Aubourg et al. 2008; Silva et al. 2004, 2008, 2010, 2014, 2018; Chadima et al. 2009; Delcamp et al. 2014; Hrouda et al. 2015).

Due to the collapse of half of the Wai'anae volcano in Hawaii (Fig. 1), the internal part of this volcano is now exposed, revealing dike swarms. For the inner part of this

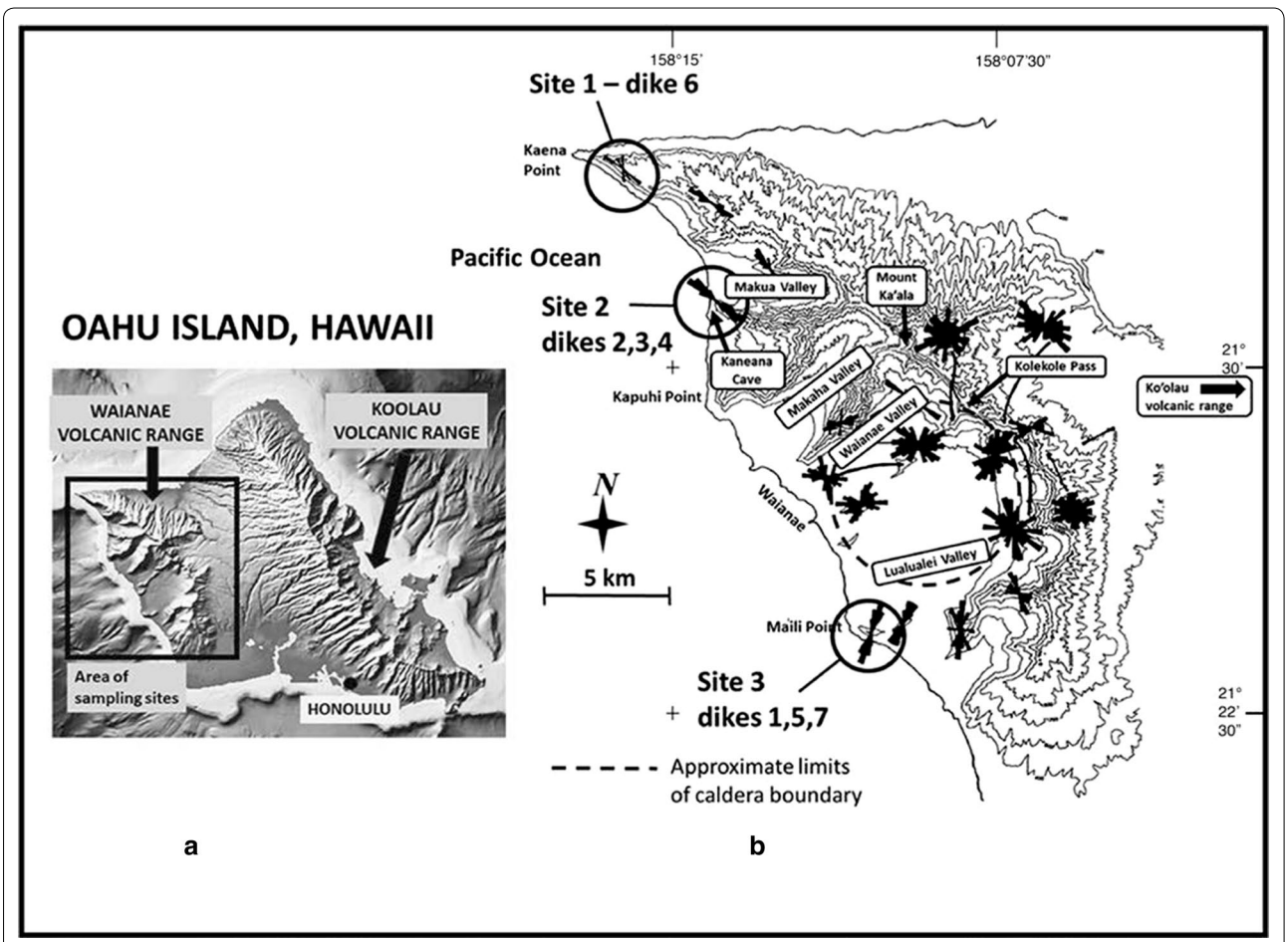

Fig. 1 **a** Simplified view of Oahu with Digital Elevation Model (NOAA—Digital Elevation Models: https://www.ngdc.noaa.gov/mgg/coastal/coastal.html) and the two main volcanic structures, the Koolau and Wai'anae volcanic ranges. The sampling sites area over the Wai'anae volcano is indicated, **b** elevation contour map of the Wai'anae volcano, dike orientations (adapted from Zbinden and Sinton 1988) and site locations of this study

volcano, studies concerning the emplacement of these dikes are aimed at providing fundamental new insights into the origin of these dikes and the flow direction of the magmas.

An AMS study of seven pilot dikes sampled inside and outside the Wai'anae caldera was then performed. It was complemented with a detailed analysis of the magnetic properties of the samples, to look for possible magnetic mineral alterations that would prevent a scientifically sound interpretation of the AMS. Knowledge of the dike flow emplacement of the seven pilot dikes in the Wai'anae volcano helps to understand the inflation and flank collapse processes that affected the volcano.

Previous geologic works

The petrology of the volcano was studied, determined and published with the original geological map by Stearns (1940) and McDonald (1940). The geology of the Wai'anae volcano has been described in detail by Sinton (1986) and briefly summarized by Herrero-Bervera and Coe (1999). The Wai'anae volcano has also been mapped by Sinton (1979, 1986) by means of structural, geochemical and lithologic tools to determine the map units. The first paleomagnetic study of the Wai'anae volcano was published by Doell and Dalrymple (1973) who provided reliable K–Ar age determinations, indicating that the subaerial volcanic activity took place before 3.8 Ma to approximately 2.4 Ma. The magnetostratigraphy and the dating of the Gauss–Gilbert, lower and upper Mammoth geomagnetic reversals were studied by Herrero-Bervera and Coe (1999) and Herrero-Bervera and Valet (1999, 2005). These radiometric and paleomagnetic studies corroborate the fact that Hawaiian volcanoes were built very rapidly, with an eruption rate averaging 1000 years as with the flows of Mauna Loa and Kilauea volcanoes. Today, we know the Mauna Loa volcano on the Big Island of Hawaii has erupted 33 times since 1843, which yields an average of one eruption every 5 years (Trusdell 2012). The first study of the dike swarms emplaced on the Wai'anae volcano was published originally by McDonald (1940) and subsequently by Zbinden and Sinton (1988). Figure 1 depicts the distribution and orientation, as well as the location of the sampling sites of the dike swarm both inside and outside the caldera.

Sampling

Seven thin pilot dikes were selected in three areas, called hereafter sites 1, 2 and 3 following a NNW–SSE transect, west of the deep internal part of the Wai'anae volcano and outside the caldera (Fig. 1). Area 1 is located close to Kaena Point at the NW limit of the Kamai'leunu Member, which is the oldest member of the Wai'anae volcanic stratigraphy within the Gauss Chron (e.g., Herrero-Bervera and Valet 2005) of the Wai'anae volcanics. The dikes in this area are usually slightly weathered and show steady directions from NW–SE to NNW–SSE. A single dike (DK6) presenting non-weathered chilled margins was sampled. Area 2, nearly 8 km southeast of Area 1 and also belonging the Kamai'leunu Member, is located in the southern border of Makua Valley. Most observed dikes show a NW–SE to WNW–ESE trend. Three dikes from this area were selected (DK2, DK3, DK4). Dikes DK2 and DK3, located close to Kaneana Cave (Fig. 1b) are parallel, E–W trending and only separated by a few meters. Field relationships suggest that several magma pulses were emplaced in these dikes. Dike DK4 is trending roughly N–S with moderate dip (i.e., 46°; Table 1). Area 3 is located in the central part of the Wai'anae volcano close to Maili Point, roughly 16 km southeast of Area 2. The dikes here show a predominant NNE–SSW trend. Three dikes (DK1, DK5 and DK7) were sampled. We note that dike DK5 has a complex shape with a local inclusion of host rocks. The average thickness of the dikes in the three areas is about 0.4 m up to 2.5 m (see Table 1).

For magnetic fabric studies, it is very important to study imbrication angles that are observable on the dike margins. Most of the samples have to be drilled on these borders (e.g., Cañón-Tapia and Herrero-Bervera 2009). The samples for this study were drilled following a geometry that resembles an "H" letter. The vertical strokes of the H, on the dikes borders, are parallel to the dike's margins with a small spacing between the samples (for analysis of the imbrication angles). The horizontal stroke of the H cuts across the dike, with a larger spacing of the drilled specimens for study of the magma flow within the dike. Letters W, M and E, associated with the name of the dike, will correspond to samples from the Western margin, Middle part and Eastern margin, respectively (DK2M for example). The drilled cores were oriented both by means of magnetic and sun compasses. Only the sun compass orientation of the samples was used for the AMS study.

Rock magnetism

In order to characterize the magnetic mineralogy and associated grain size of the studied dikes, several rock magnetic experiments have been performed. These data are key information for the magnetic fabric interpretation. The eventual presence of several magnetic minerals and/or magnetic grains with different sizes is factors that can significantly affect the AMS.

Magnetic susceptibility experiments

The mean susceptibility [$K_m = (K_1 + K_2 + K_3)/3$] has been calculated from the AMS data that will be presented in "Anisotropy of magnetic susceptibility (AMS) determinations" section. The average value of the mean

Table 1 Geometry of the dikes and mean AMS data

Area	Dike #	Dike thickness (m)	Dike orientation strike (°)/dip (°)	MZA D (°)/I (°)	Site	*n*	K_m 10^{-3} SI	*K*1 D (°)/I (°)	*K*3 D (°)/I (°)	*P′*	*T*	Fabric type
1	DK6	2.5	145/90W		DK6W	23	36.8	88/52	315/28	1.007	0.20	Int
					DK6 E	16	37.4	102/83	356/2	1.011	− 0.07	Int
2	DK2	2.5	96/85S	119/24	DK2W	5	36.3	256/58	113/26	1.011	0.63	Int
					DK2WL	6	19.3	272/61	121/25	1.015	0.47	Int
					DK2M	16	35.5	298/60	31/2	1.012	0.71	N
					DK2E	5	39.5	111/15	201/3	1.015	0.34	N
	DK3	2	96/85S	143/23	DK3W	12	23.4	330/43	114/41	1.007	− 0.35	Int
					DK3M	10	6.6	222/82	48/8	1.009	− 0.07	N
					DK3 E	13	20.5	38/11	133/24	1.013	− 0.08	Inv
	DK4	0.8	352/46E	71/61	DK4W	10	2.8	97/74	247/13	1.005	0.44	N
					DK4M	7	3.1	98/55	256/33	1.007	0.50	N
					DK4 E	12	2.7	113/61	238/18	1.005	− 0.26	N
3	DK1	1	15/90	181/74	DK1W	5	11.6	214/68	308/0	1.008	0.29	N
					DK1M	11	9.8	186/69	322/16	1.012	− 0.88	N
					DK1 E	7	11.9	184/71	87/2	1.009	0.63	N
	DK5	0.4	350/90	177/35	DK5W	13	2432	242/50	357/20	1.002	− 0.10	N
					DK5M	5	2335	323/66	83/13	1.003	− 0.35	N
					DK5 E	8	3560	169/27	265/11	1.008	− 0.38	N
	DK7	0.5	190/52W	208/6	DK7W	14	5817	264/32	114/41	1.009	0.77	N
					DK7M	8	5874	241/29	48/8	1.007	0.40	N
					DK7 E	12	7573	24/30	133/24	1.005	0.03	N

MZA magnetic zone axis, K_m mean susceptibility, K_{max} maximum susceptibility, K_{min} minimum susceptibility, *D* and *I* declination and inclination of the axes, respectively, *P′* and *T* corrected anisotropy degree and shape parameter of Jelinek (1981), *Int, N and Inv* intermediate, normal and inverse magnetic fabric, respectively

susceptibility for all dikes is $15.5 \pm 13.8\ 10^{-3}$ SI units, corresponding to a large scatter in susceptibility values for the sample scale with a bimodal distribution (Fig. 2d), indicating possibly heterogenous magma sources in two populations of samples. Dikes DK4, DK5 and DK7 show low mean susceptibility values ($K_m < 10 \times 10^{-3}$ SI). Dikes DK2 and DK6 display the highest susceptibilities ($K_m > 30 \times 10^{-3}$ SI) and dikes DK1 and DK3 have intermediate susceptibilities (Fig. 2a). The susceptibility variation across the dikes is diverse according to the studied dikes. In dikes DK1, DK2, DK3 and DK5, the mean minimum K_m occurs in the middle of the dike. Moreover, on the western margin of DK2, the six samples, close to the margin, show susceptibility values about half that of the other samples of this dike. No particular indication of stronger weathering (see Krasa and Herrero-Bervera 2005) appears in these samples. They could therefore correspond to another intrusive phase or to local contamination by melted xenoliths. It is also possible that the K_m is lower due to an heterogeneity of the magma, i.e., a heterogeneous distribution of the magnetic minerals. These six samples will be considered separately in this paper and referred to as site DK2WL. For the two non-vertical dikes (i.e., DK4 and DK7), the minimum mean susceptibility corresponds to the upper part of the dikes. The susceptibility variation across each dike is weak, except in DK3 where samples from the center of the dike show values of susceptibility much lower than those close to the margins (Fig. 2a). Such a strong variation indicates a very heterogeneous body, possibly reflecting multiphase intrusions. For dikes yielding weak susceptibility variation between the core and margin (e.g., DK4, DK5 and DK7), the variation could correspond to slightly different grain sizes related to faster cooling on the dike border and/or to slightly different weathering degrees in the different parts of the dike.

Thermomagnetic *K*(*T*) curves

Continuous and partial thermomagnetic cycles of low-field magnetic susceptibility versus temperature *K*(*T*) curves were determined for different samples, at least one for each studied dike (curves are shown on Fig. 3 for three selected samples). The experiments were performed in a CS4 furnace coupled to a MFK1-FA Multi-Function Kappabridge, operating at a low field of 200 A/m and a frequency of 976 Hz. The susceptibility was measured from room temperature up to a maximum of 620 °C, with a heating and cooling rate of 9 °C/min, and under an Argon

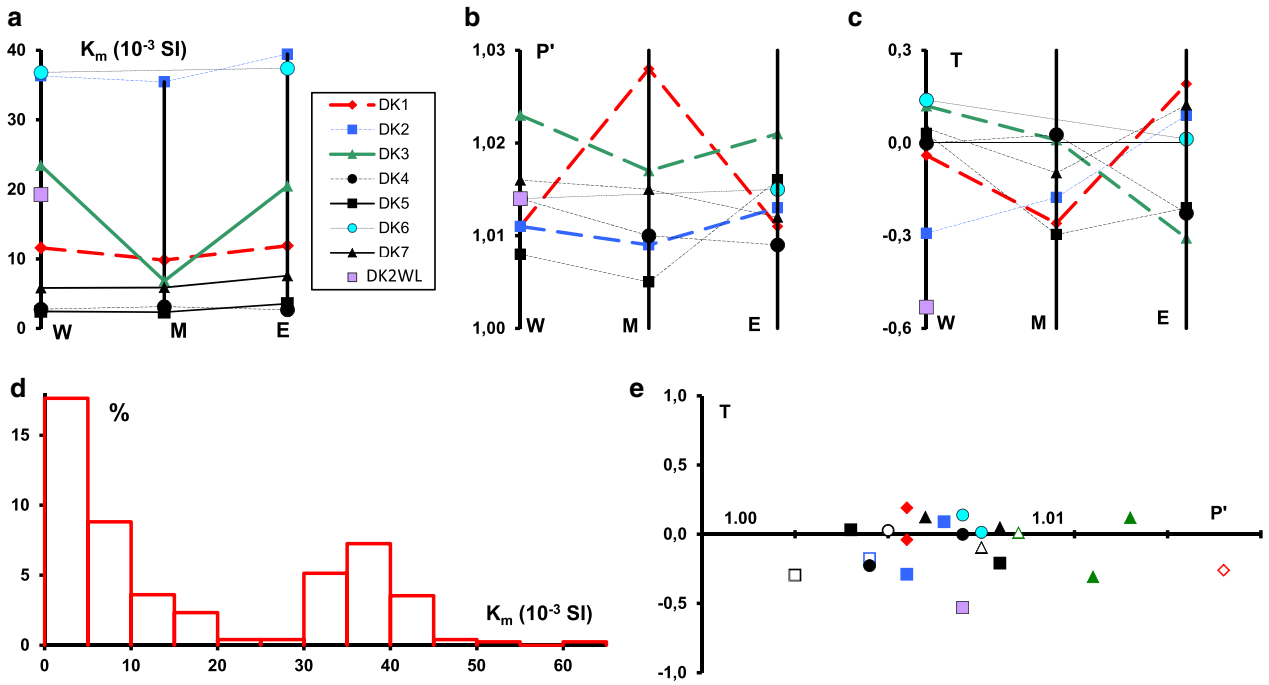

Fig. 2 AMS scalar parameters. **a**–**c** Mean values of K_m (in 10^{-3} SI): P', and T in the western (W), middle (M) and eastern (E) parts of the studied dikes, **d** distribution of K_m for all the specimens, **e** $P'T$ diagram (Jelinek 1981) for mean values in different parts of the dikes (full squares and open symbols correspond to the marginal and central parts of the dikes, respectively; see **b**, **c** for details)

atmosphere using the instrument at the Petrofabrics and Paleomagnetics Laboratory of HIGP-SOEST of the University of Hawaii as well as an identical instrument at the Instituto Dom Luís (Lisboa), Portugal.

The Curie temperature (T_c) was estimated according to the Petrovský and Kapicka (2006) approach, which proposes that, if a sharp Hopkinson peak is present, the temperature corresponding to the peak is a good estimate for the Curie temperature. However, the $K(T)$ curve shows a wide maximum with a smooth increase and decrease in the susceptibility over a large temperature range. The best estimate for the Curie temperature should then be then the temperature of the observed inflection point in the decreasing branch of susceptibility.

All samples show irreversible $K(T)$ curves (Fig. 3a, d, g), which indicate the occurrence of mineral alterations during the heating phase (hereafter called "first" cycle). A "second" heating–cooling cycle was performed in all samples with the powder already used in the previous cycle. The heating–cooling curves of these second cycles show a practically reversible process as observed in the sample from DK2 (Fig. 3h), or very similar paths as observed in the samples from DK7 and DK3 (Fig. 3b, e).

"Partial" thermomagnetic cycles of $K(T)$ were also performed for all samples. For each partial cycle, the powder that had been processed in the previous lower temperature cycle was used. These experiments revealed reversible behavior of the susceptibility heating and cooling curves for temperatures lower than 250–300 °C (Fig. 3c, f). The low-temperature hump ($T<300$ °C), observed during the heating process in all samples except sample from DK2, is then related to a stable magnetic component that is not altered during heating up to 300 °C. With increasing temperature, another hump is observed between 450 and 500 °C in "first" (Fig. 3a, d, g), as in partial cycles (Fig. 3c, f, i). All $K(T)$ curves up to 610 °C (first, second, and partial cycles) yield a Curie temperature $T_c=560$ °C, but that could correspond to a primary mineral as well as a magnetic phase resulting from mineral alteration during the heating. For temperatures above 575–610 °C, all samples show virtually zero magnetic susceptibility. The cooling curve is complex, showing multiple phases, and the final magnetic susceptibility of the first cycles, after the cooling process, is always slightly higher than the initial magnetic susceptibility before the heating (Fig. 3a, d, g). A sample from DK2 (Fig. 3g) shows a different behavior with a continuous (hyperbolic type) rise of the $K(T)$ heating curve up to a sharp peak that occurs at 480 °C, followed by an abrupt decrease in susceptibility. The cooling curve for the partial loop up to 510 °C suggests that this decrease is related to mineralogical alteration and that the sharp

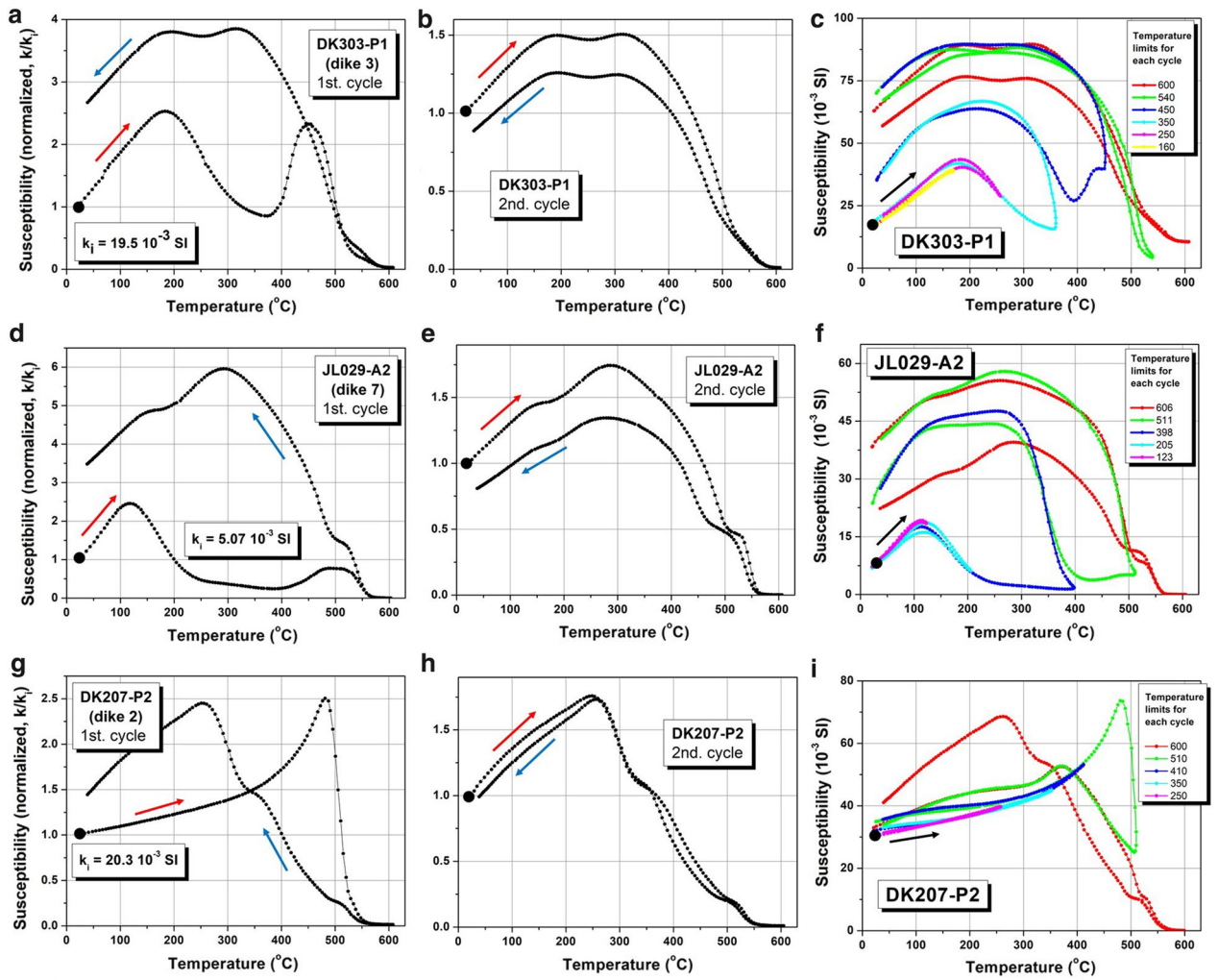

Fig. 3 Selected plots of magnetic susceptibility versus temperature (*T*) for three samples DK3 (above), DK7 (in the middle) and DK2 (below). First, heating–cooling cycles (left plots, **a**, **d, g**) and second heating–cooling cycles (central plots, **b**, **e**, **h**). The susceptibility values are normalized relative to the initial susceptibility at room temperature (ki, given on the left diagram). Right plots (**c**, **f**, **i**) show the partial heating–cooling cycles

peak at 480 °C during heating is not related to the Hopkinson effect (e.g. Herrero-Bervera and Valet 2009) . All other samples (Fig. 3a–d) show a Hopkinson peak at temperatures between 90 and 180 °C. With increasing temperature, mineralogical alteration occurred after 300 °C heating.

An interesting observation can be made from partial $K(T)$ curves (Fig. 3c, f). For cycles with a maximum temperature between 300 and 510 °C, the susceptibility strongly increases before the cooling beginning, showing an unexpected appearance of mineralogical alteration due to cooling. This is actually partially related to the relatively fast heating rate (Jordanova and Jordanova 2016), but also because the minerals formed during heating have Curie temperatures lower than the temperature during their formation. Such behavior clearly appears on the subsequent cycles with a higher maximum temperature, where the heating curve is similar to the cooling curve of the previous cycle. This highlights the major interest of the partial $K(T)$ experiments (e.g., Henry 2007).

The analysis of the thermomagnetic curves suggests that most samples display a mixture of magnetic phases.

- One phase is revealed by the low-temperature Hopkinson peak observed in the $K(T)$ curves and should be a Ti-rich titanomagnetite. Indeed, titanomagnetites (Fe_{3-x} Ti_x O_4) of the TM60 composition (stoichiometric for $x=0.6$) have Curie temperatures of

≈150–200 °C. On samples from DK1, DK3 (Fig. 3a), and DK4, the estimated values of T_c around 225–250 °C point to a titanomagnetite with $x \approx 0.4$, while for DK5 the lowest value of $T_c \approx 160$ °C suggests a value of $x \approx 0.6$. These minerals are clearly primary, as evidenced by the reversibility of the $K(T)$ curves for low temperatures.

- After heating at temperatures higher than 250 °C, the cooling curves (first, second and partial heating–cooling cycles) show a susceptibility increase, which indicates the formation of a mineral of high susceptibility. The partial $K(T)$ experiments show that the newly formed minerals correspond to a wide spectrum of Curie temperatures. That suggests conversion of titanomaghemite into titanomagnetite possibly associated with an exsolution phenomena and grain size variation. A second magnetic phase in our samples should therefore be titanomaghemite.
- A third phase is associated with the high-temperature reversible variations that results in Curie temperatures of 525–550 °C, and points to the contribution of Ti-poor titanomagnetite, possibly produced from the conversion of Ti-poor titanomaghemite (Dunlop and Özdemir 1997).

IRM/SIRM acquisition curves

Uniaxial isothermal remanent magnetization (IRM) was induced in four specimens (one sample per dike for DK2, DK5, DK6 and DK7). The specimens were first demagnetized by an alternating magnetic field at 100 mT. Magnetization measurements were performed with an AGICO JR-6 Spinner Magnetometer at regular intervals when samples were further submitted to a progressive uniaxial increasing DC magnetic field up to 1.2 T (saturation of isothermal remanent magnetization—SIRM—acquisition), and later when they were submitted to a progressive uniaxial increasing DC magnetic field in the opposite direction of the previous SIRM (back-field "demagnetization"). Fields were applied with an ASC Scientific IM-10-30 Pulse Magnetizer. The obtained IRM acquisition curves and associated backfield demagnetization curves provide information on the magnetic mineralogy. Low-coercivity phases such as magnetite, maghemite, greigite or ferromagnetic pyrrhotite grains are characterized by saturation for low applied fields (< 0.3 T). Higher coercivity phases such as hematite, goethite, and ferrimagnetic pyrrhotite (which reach saturation field of ~ 500 mT and not higher than 1.0 T) do not reach saturation until fields higher than 1.0 T. Moreover, the SIRM intensity gives an indication about the relative concentration of these magnetic minerals in a given volume. According to Robertson and France (1994) and Kruiver et al. (2001), the IRM acquisition curves theoretically follow a log-normal distribution and are cumulative in intensity. The obtained magnetization curves can therefore be described by three main parameters: (1) SIRM intensity; (2) field at which half of the SIRM is reached ($B_{1/2}$); and (3) a dispersion parameter (DP), which reflects the distribution of the coercivities of the magnetic mineral phases and characterizes the homogeneity of the population in terms of grain size and composition. The IRM acquisition process can be visualized in a diagram with the log applied field in the abscissae scale and the magnetization acquisition or the gradient magnetization acquisition in a linear ordinate scale, referred to as LAP (for the linear acquisition plot) or GAP (for the gradient acquisition plot) diagram. These diagrams reveal the occurrence and contribution of magnetic components with different coercivities (i.e., different "stages" in the IRM acquisition curve) and the heterogeneity of the magnetic assemblage of phases (width and overlapping of the peaks) in the total IRM. In our samples, results show small differences including saturation being reached in fields lower than 0.4 T, and even lower than 0.2 T for one sample (Fig. 4a). The remanent coercive force (H_{CR}), obtained from the backfield demagnetization curves, has low values, varying from 19 to 50 mT (Fig. 4a, inset). The SIRM intensities show also small variations, spanning between 300 and 750 A/m.

The LAP and GAP (Fig. 4b, c) reveal two components: one of low coercivity (25 mT < $B_{1/2}$ < 56 mT) that usually represents 95% of the total coercivity, and the other component of higher coercivity (100–300 mT) representing only 5% of the total coercivity (only the sample from DK7 shows a slightly different high coercivity contribution reaching 19%). That could correspond to titanomagnetite and titanomaghemite, respectively.

Hysteresis properties and magnetic grain size determination

To determine hysteresis parameters (Mrs, Ms, Hcr and Hc) and magnetic grain sizes, we prepared powder samples of approximately 200 mg of seven specimens representative of the seven studied dikes. The hysteresis loop measurements were performed on a variable field translation balance (VFTB) with a measuring range of 10^{-8}–10^{-2} A/m of the Petrofabrics and Paleomagnetics Laboratory of the HIGP-SOEST, University of Hawaii.

A wasp-waisted shape appears at least for part of the obtained curves, confirming the presence of several magnetic phases. As depicted by the magnetic granulometry diagram (Day et al. 1977) modified by Dunlop (2002) presented in Fig. 5. Only specimen number 5 should be of SD size (the sample shows a high coercivity with respect to the other wasp-waisted specimens, see Additional file 1). Most grain sizes are scattered

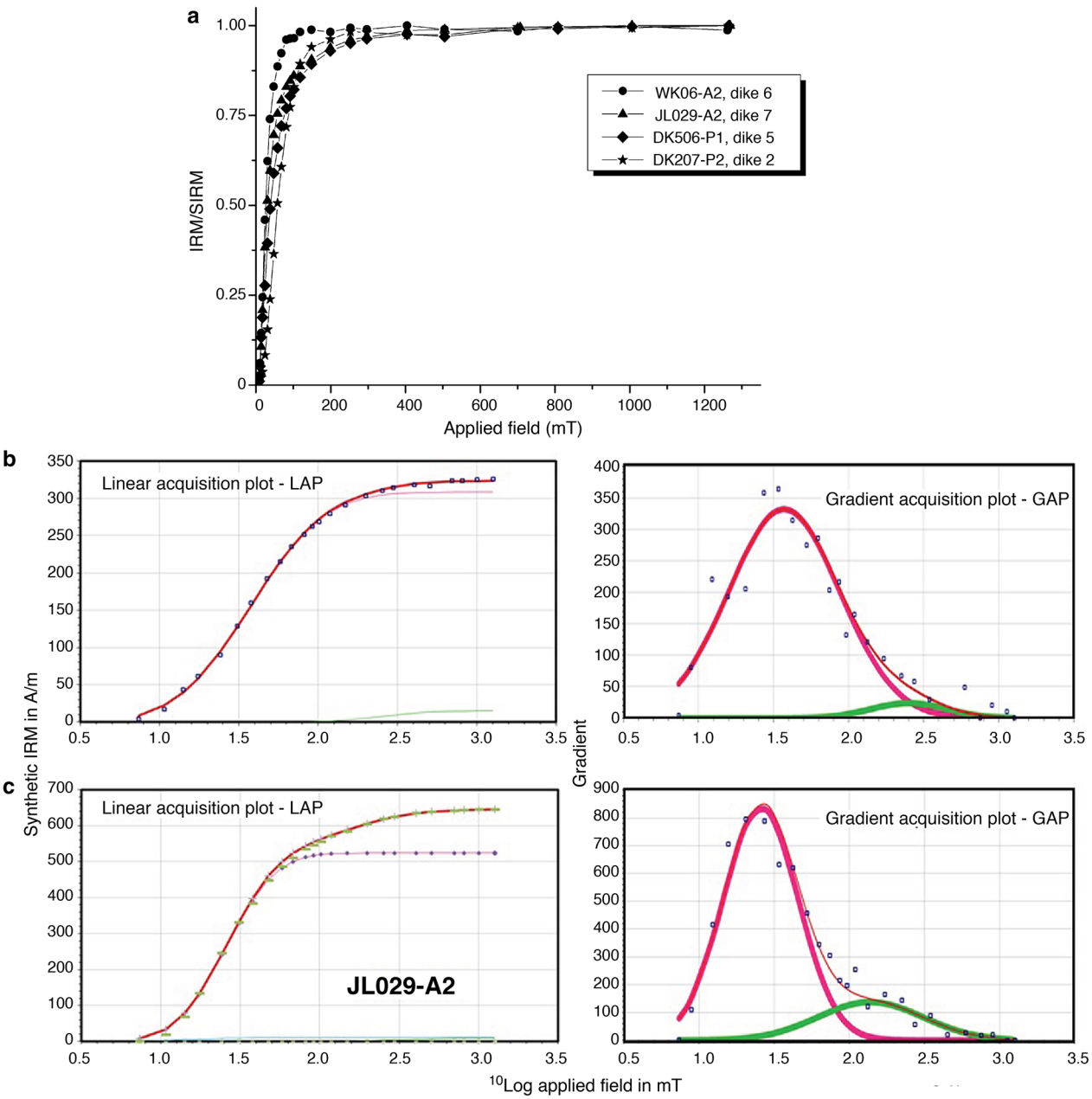

Fig. 4 IRM/SIRM acquisition curves. **a** Plot of IRM acquisition and backfield demagnetization curves (inset) for four representative samples, **b**, **c** linear acquisition plot (LAP) and gradient acquisition plot (GAP) for two representative samples

within the PSD range, close to the mixing curves between SD and Multi-Domain (MD) grains. The presence of both SD and larger grains suggests the presence of both normal and inverse fabrics (e.g., Potter and Stephenson 1988; Rochette 1988; Hrouda and Ježek 2017; see also Table 1), possibly resulting in composite "abnormal" fabrics. It is, however, very important to point out that domain limits in this plot apply to pure magnetite only. In our case, magnetic mineralogy corresponds to at least two phases, including titanomaghemite and Ti-rich titanomagnetite. The analysis of the thermomagnetic curves suggests that most samples display a mixture of magnetic phases resulting in a variety of different magnetic fabrics.

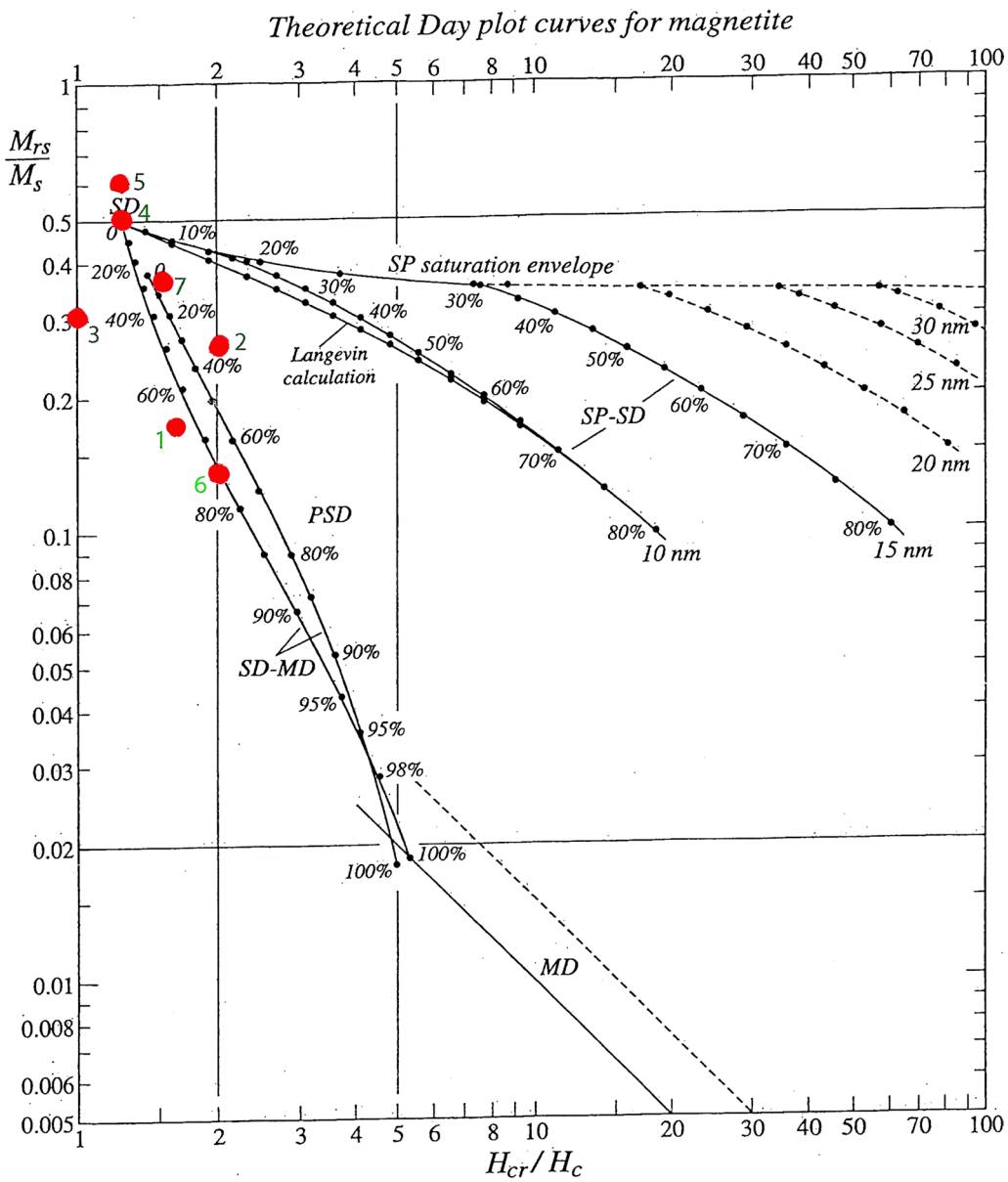

Fig. 5 Results of the hysteresis experiments performed on seven representative samples displayed in a Mrs/Ms versus Hcr/Hc, Day plot with limits between single domain (SD), pseudo-single domain (PSD) and multi-domain (MD) grains after Dunlop (2002). The figure also shows mixing curves calculated for magnetite using the equations developed by Dunlop (2002). Numbers along the curves are volume fractions of the soft component (SP or MD) in mixtures with SD grains. The dikes analyzed are DK1; DK2; DK3; DK4; DK5; DK6 and DK7. The plot shows green numbers 1, 2, 3, 4, 5, 6 and 7 corresponding to the seven dikes studied

Anisotropy of magnetic susceptibility (AMS) determinations

The AMS measurement yields a susceptibility ellipsoid of principal susceptibility axes K_{max}, K_{int} and K_{min} ($K_{max} \geq K_{int} \geq K_{min}$) and mean susceptibility $K_m = (K_{max} + K_{int} + K_{min})/3$. Therefore, the intensity and shape of this ellipsoid are characterized Jelinek's (1981) parameters P' and T. The parameter P' (corrected degree of anisotropy) is, at the grain scale, controlled by the geometry and orientation of the crystallographic system. P' expresses the departure from a spherical AMS ellipsoid ($P'=1$). The degree of anisotropy measures the strength of the preferred orientation of the magnetic minerals in a rock. The parameter T characterizes the shape of the AMS ellipsoid. If $0<T<+1$ the AMS ellipsoid is oblate (the magnetic fabric is planar); $T=+1$

means that the AMS ellipsoid is rotationally symmetric (uniaxially oblate). If $-1 < T < 0$ the AMS ellipsoid is prolate (i.e., the magnetic fabric is linear); $T = -1$ means that the AMS ellipsoid is uniaxially prolate (e.g., Hrouda et al. 2015).

Measurements of AMS were made on KLY2 Kappabridge (AGICO, Brno) at the Petrofabrics and Paleomagnetics Laboratory of the Hawaii Institute of Geophysics and Planetology (HIGP), School of Ocean and Earth Science and Technology (SOEST), University of Hawaii at Manoa. The interpretation of the magnetic fabric at the site scale was done using the bivariate statistics with weighting by the measurement of the k precision parameter (Fisher 1953) values, therefore integrating the measurement uncertainty (Henry and Le Goff 1995), and the classical normalized tensor variability statistics (Hext 1963; Jelinek 1978).

Magnetic fabric in dikes

Today, it is well known that it is possible to identify in volcanic rocks, the predominant magnetic mineral phases (i.e., very small percentages of ferromagnetic minerals) that often control the measured magnetic fabric of mafic rocks (e.g., Stacey 1960; Khan 1962).

A good correlation between the orientation of the magnetic fabric and shape-preferred orientation of minerals, as observed in thin sections has been found in various rocks (e.g., Khan 1962; Grégoire et al. 1998). In addition, Knight and Walker (1988), who studied mafic dikes from the collapsed Koolau volcano (Oahu, Hawaii), confirmed the agreement between the orientation of the principal axes of AMS and macroscopic flow related structures (such as surface lineations consisting of parallel, millimeter-high wrinkles projecting out from the weathered chilled margins and cross sections that show imbricated sheet joints along dike margins (see for example Knight and Walker 1988, figure 3). Mafic dikes on the Isle of Skye, from the highly dissected Cuillin Hills magmatic center, also corroborate the agreement between orientation of the AMS principal axes and structures related to magma flow (Herrero-Bervera et al. 2001).

Rochette et al. (1991, 1999) and Tauxe et al. (1998) found that it is possible to distinguish between "normal" and "abnormal" magnetic fabrics of dikes. They defined the normal magnetic fabric as characterized by a mean minimum axis K_{min} subperpendicular to the dike wall (Fig. 6a). An abnormal fabric could have a primary origin, related to mixtures of the different grain types (Soriano et al. 2016), to interaction of particles during dike emplacement (e.g., Aifa et al. 1999; Dragoni et al. 1997; Cañón-Tapia 2004; Cañón Tapia and Chávez Álvarez 2004; Schöbel and de Wall 2014), or be due to the presence of SD magnetite, giving, in this case, an inverse fabric (e.g., Potter and Stephenson 1988; Ferré 2002; Silva et al. 2008; Schöbel and de Wall 2014; Hrouda and Ježek 2017). Inverse fabric is characterized by mean maximum axis K_{max} subperpendicular to the dike wall (Fig. 6b). The presence of both MD and SD grains of magnetite can give composite or intermediate fabric, which is between normal and inverse fabrics (Fig. 6c) (Rochette et al. 1999; Ferré 2002). A secondary origin could be related to post-emplacement modification of the fabric during cooling or under the effect of tectonic strain (Henry 1974; Ellwood 1978; Park et al. 1988). Knight and Walker (1988) founded that, along the dike margins, there is commonly an imbrication angle between magnetic foliation and the dike walls, reflecting the tilting of mineral particles (Fig. 6). The Isle of Skye dikes also showed such an imbrication (Herrero-Bervera et al. 2001). Since the work of Knight and Walker (1988), the K_{max} in dikes was often used to infer the magma flow direction. However, like in lava flows (Cañón-Tapia et al. 1995, 1996; Henry et al. 2003), K_{max} is not always parallel to the assumed flow direction, as shown by Geoffroy et al. (2002) who proposed to use the imbrication of the magnetic foliation to infer the flow vector in dikes (Figs. 6, 7). The flow direction is in the dike plane, perpendicular to the intersection between magnetic foliation and the dike margin; the sense of magma motion is given by the orientation of the imbrication angle that points in the same direction as the magma flow (Fig. 7). Callot and Guichet (2003) applied this methodology in dikes from the Greenland volcanic margin and confirmed that the K_{max} is not always parallel to flow direction. The magnetic zone axis (Henry 1997) represents the best intersection of the magnetic foliation measured in different samples from the same site. As for the imbrication angle, it is a good indicator of the direction perpendicular to the flow direction [see Fig. 7(1), (2), (3)].

Application to Hawaiian dikes: the Wai'anae volcano case

In the data set obtained in the present pilot study, there is a relatively good agreement between the results of the bivariate (Figs. 8, 9, 10, 11; Henry and Le Goff 1995) and normalized tensor variability (Table 1; Hext 1963; Jelinek 1978) statistics, indicating homogeneous measurement uncertainty in most samples. To obtain information about the imbrication, the results from each margin and the middle part of the dikes are considered as three independent sites: western (W), middle (M), and eastern (E). Within each of these sites, we retained only data calculated with the neighboring mean susceptibility values. Therefore, few data with very large measurement uncertainty were rejected. The anisotropy is weak, with mean P' values mostly between 1.01 and 1.02, reaching a maximum value of 1.05 in very few samples (Table 1; Fig. 2b).

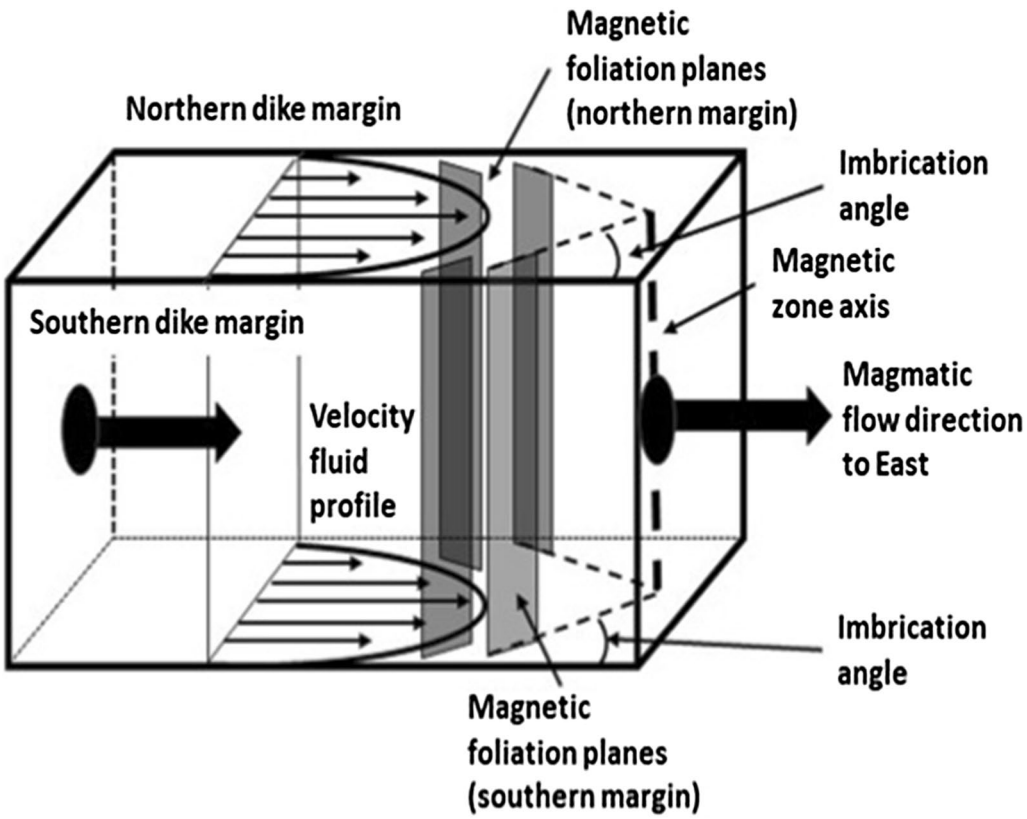

Fig. 6 Determination of the flow direction in dikes using magnetic imbrication angles. Assuming a Newtonian laminar flow without along-plane displacement of the borders (mode I dike of Knight and Walker 1988), near a dike margin, the flow induces a strain regime characterized by simple shear. So, even with low particle concentrations the phenocrysts would interact and align their long axis predominantly along with the flow direction, in a plane parallel or making a small imbrication angle with the dike margin. Magnetic particles that form and develop between the phenocrysts will replicate the orientations and alignments of the phenocrysts. Considering a normal magnetic fabric, the magnetic foliation planes near the borders will be coincident with the particle's imbrication planes. Therefore, the flow sense can be specified for cases with clearly visible imbrication on both dike borders

The susceptibility ellipsoid is mostly slightly oblate (Table 1; Fig. 2e) and the fabric in several dikes is more prolate in the middle part than close to margins (Fig. 2c). Uncertainty on the mean orientation of the axes is relatively large (Figs. 8, 9, 10), as is the case in these lava flows (e.g., Cañón-Tapia et al. 1995, 1996; Hrouda et al. 2015).

A major constraint could be given by the possible presence of SD magnetite grains (Fig. 5), which opens the possibility that inverse fabric plays a significant role in the measured AMS (Fig. 6b). Figures 8, 9 and 10 show that a normal fabric was obtained in most samples of all sites, except for dikes DK2W, DK2WL, DK3W, DK3E, DK6W and DK6E (all corresponding to the dike margins). These abnormal fabrics correspond to an inverse fabric clearly only at site DK3E and to intermediate fabrics in the other cases. The superposition of normal and inverse fabrics probably explain the low anisotropy in most samples (Hrouda and Ježek

(See figure on next page.)

Fig. 7 Conceptual block diagrams and Schmidt (equal area) plots (maximum K_{max}, intermediate K_{int} and minimum K_{min} axes represented by squares, triangles and circles, respectively; projection on the lower hemisphere showing different relationships between crystal orientation, magma flow direction, and principal susceptibilities). The blocks represent a section of a north–south vertical dike with vertical upward magma flow direction. The equal area plots are from the eastern dike margins. For realism, it is considered that the crystal orientations show some, but limited, scattering around a mean direction. **a** "Normal" fabric K_{max} on the Schmidt plot corresponds to the magnetic zone axis. **b** "Inverse" fabric related to the presence of SD grains. **c** Rolling effect of large grains with K_{max} oriented normal to flow direction (within the plane of the dike, K_{int} and K_{min} are parallel to flow direction according to the Fig. 6). Original diagrams are from Cañón-Tapia (2004)

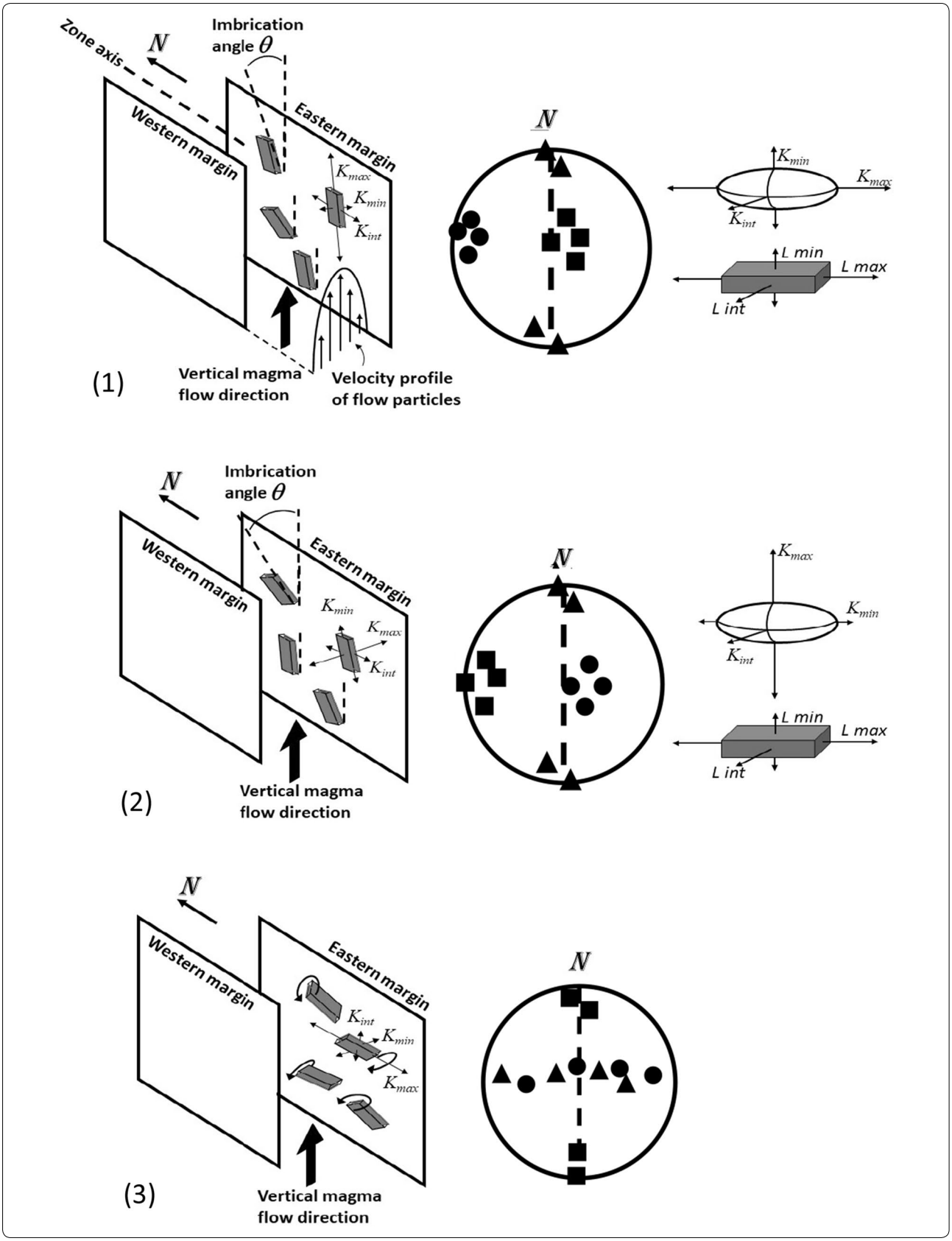
Zone axis
N
Imbrication angle θ
Western margin
Eastern margin
K_{max}
K_{min}
K_{int}
Vertical magma flow direction
Velocity profile of flow particles
(1)
N
K_{min}
K_{max}
K_{int}
L min
L max
L int
N
Imbrication angle θ
Western margin
Eastern margin
K_{min}
K_{max}
K_{int}
Vertical magma flow direction
(2)
N
K_{max}
K_{min}
K_{int}
L min
L max
L int
N
Western margin
Eastern margin
K_{int}
K_{min}
K_{max}
Vertical magma flow direction
(3)
N

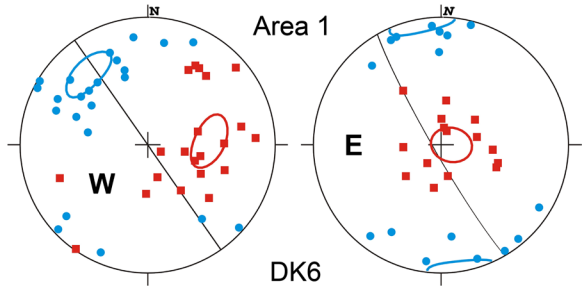

Fig. 8 AMS stereoplots for dike DK6 (Area 1). Maximum (blue squares) and minimum (red circles) susceptibility axes with confidence zone at 95% (Henry and Le Goff 1995) at the western (W) and eastern (E) margins of the dike. Orientation of the dike plane is indicated by a great circle (Schmidt diagrams, lower hemisphere

2017). Surprisingly, on the Day plot (Fig. 5), the normal fabrics correspond to samples (except from DK1) with highest amount of SD grains and the abnormal fabrics to those with more MD grains, i.e., a relationship opposite to what is expected. This clearly indicates that a factor, different from the only presence of both SD and MD grains according to the Day et al. (1977) diagram, has here a role for the type of fabric. In our dikes, magnetic mineralogy corresponds to at least two phases, including titanomaghemite and titanomagnetite. Moreover, the presence of superparamagnetic (SP) grains is also possible. Some samples, in particular those with dominant SD size on the Day plot, display wasp-waisted hysteresis loops, confirming that contain several magnetic phases. The classical interpretation of the Day et al. (1977) plot (see Dunlop 2002) about grain size could be inappropriate for our samples. However, grain sizes could be not homogeneous within a dike (on the Day diagram (Fig. 5), the two samples taken far away from the dike border, such as from dikes DK1 and DK2, have clearly PSD grain size, suggesting a cooling rate effect on grain size). Similar cases have been already encountered (see discussion in Soriano et al. 2016). That will be the subject of further studies, in particular with anisotropy of anhysteretic magnetization (AARM) determination.

Note that the orientation of the principal minimum axes is very close to the dike plane in sites DK2W and DK2WL That suggests emplacement at the same time, and then that K_m difference between these two sites could be due to contamination of DK2WL magma by fully melted local xenoliths. In DK6, a relative symmetry pertaining to a horizontal direction appears for the K_{min} axes, suggesting a possible permutation of K_{min}–K_{int} axes. However, K_{int} axes are too scattered to be used instead of K_{min} to highlight an imbrication.

Discussion

AMS and implications for flow direction in the Wai'anae dike swarms

In the studied dikes, the difference in orientation of the magnetic foliation from one side of the dike to the other is mostly small, and the uncertainty on the orientation of the principal axes is large, which makes the determination of the flow direction from the simple comparison of the imbrication angle difficult. Therefore, a statistical approach is important to analyze the AMS data. For that reason, we determined the magnetic zone axis, with confidence zones at 95 and 63% (from 10,000 bootstrap samplings; Henry 1997), for each dike. To take into account the probable superposition of normal and inverse fabrics, a criterion was first applied to reject data with a clearly abnormal fabric: Sample data corresponding to angular differences between the minimum axis and the dike plane lower than 45° were not retained for determination of the zone axis. Following this criterion, for DK6, very few data represent a normal fabric, and the magnetic zone axis could not be determined.

Figure 11 presents the magnetic zone axis obtained for each dike. Confidence zones are relatively small in DK1, DK3, and DK4, but have an elongate shape in DK2 and DK5. Magnetic zone axes have a weak plunge in DK2, DK3, and DK7 (<25°) and a steep plunge in DK1 (74°; Table 1). The magnetic zone axes have a similar orientation in neighboring DK2 and DK3. In the four dikes where K_{max} axes have a relatively coherent orientation, the magnetic zone axis is roughly parallel to the K_{max} axis (DK1) or perpendicular to this axis (DK2, DK4 and DK5).

Following the same selection criterion, confidence zones for minimum axes were determined (Fig. 11). In dikes DK2 and DK3, one of the margins did not give reliable results and the magnetic zone axis is actually mainly related to data from one margin and the middle dike area. In dikes DK1 and DK4, the difference between the confidence zones for the minimum axes concerns the declination, indicating a weak plunge in the flow direction. Observed imbrication allows to specify that the latter is slightly downward toward the north in DK1 and upward toward the same direction in DK4. In dikes DK5 and DK7, the difference between the confidence zones is related to inclination, which highlights a steeply plunging flow direction. In both cases, the imbrication shows that the flow is downward. All of these data suggest inflation (locally favoring downward backflow of the magma, e.g., Silva et al. 2010) of this inner part due to magma accumulation The flow sense is unclear in the other sites due to the large scattering and the presence of abnormal fabrics.

Formation of dikes within a volcano implies opening of new spaces that are filled by magma, i.e., an accumulation

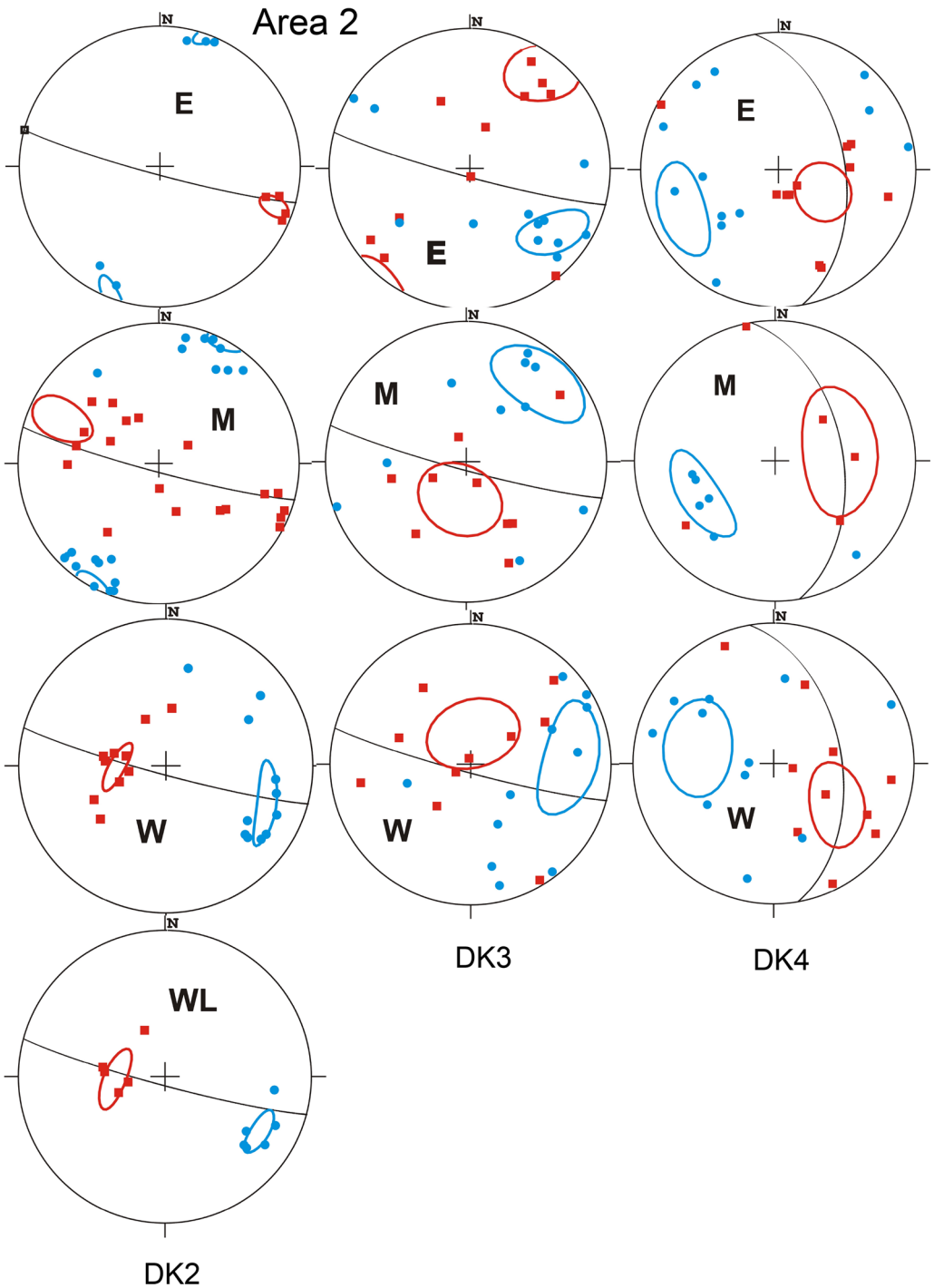

Fig. 9 AMS stereoplots for dikes DK2, DK2L, DK3 and DK4 (Area 2). Same symbols as indicated in Fig. 8. *M* middle part of the dikes

of new magma (e.g., Yang and Davis 1992). Such magma accumulation at different levels of central part of a volcano is favored by steep flow direction (feeding from below) within dikes (dikes DK2, DK3, DK5 and DK7), but here also by subhorizontal flow in dikes DK1 and DK4 toward the inner part of the volcano (Figs. 1, 11). All of these data suggest inflation of this inner part due to accumulation of new magma, from below but also from a lateral feeder, causing subsequent destabilization, and flank collapse of the Wai'anae volcano.

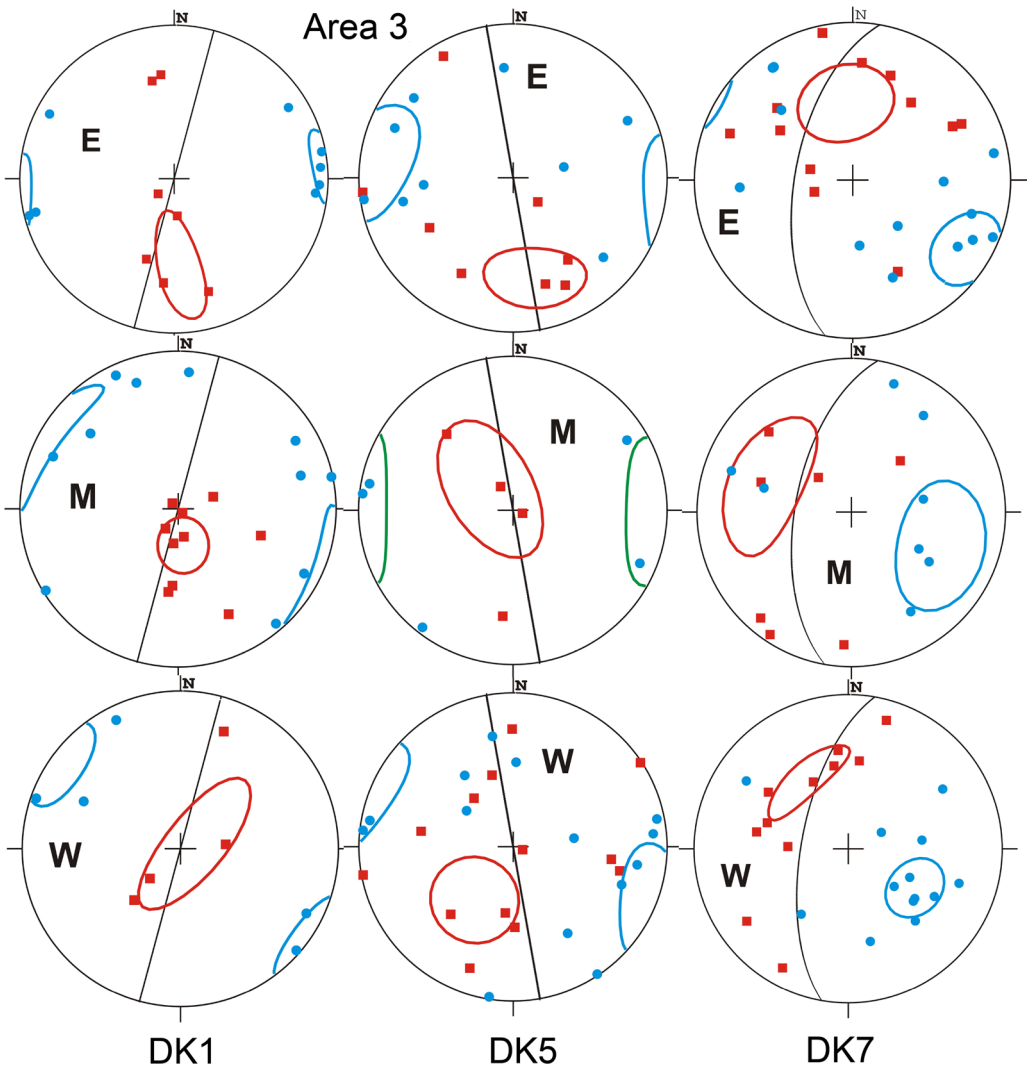

Fig. 10 AMS stereoplots for dikes DK1, DK5 and DK7 (Area 3). Same symbols as indicated in Fig. 8. *M* middle part of the dikes

Conclusion

Magnetic fabric is a very strong tool for the analysis of the emplacement conditions of dikes within a volcano. Our sampling strategy (i.e., large number of samples and location of most of the samples at dike margins) is a key to the understanding of the Wai'anae volcano dike petrofabrics and magmatic flow directions. Thanks to this strategy, and despite the small number of studied dikes, our analysis yielded important and meaningful results that improve our volcanological understanding of the destabilization and flank collapse of the entire Wai'anae volcano. Alteration may deeply modify the magnetic fabric of dikes (see Krasa and Herrero-Bervera 2005). In the present study, magnetic experiments show that most samples have retained part of their original magneto-mineralogical composition, allowing reliable AMS data. Part of the latter are, however, abnormal fabrics, likely related to the presence of several magnetic phases. We used a simple criterion to eliminate most of the abnormal fabrics, in order to keep only reliable data. That allowed a better way to interpret the data.

The results indicated dominantly vertical magma movements around the central parts of the Wai'anae volcano. This caused inflation in this portion of the volcano. This process of dike emplacement in the Wai'anae volcano is one of the endogenetic factors that has greatly contributed to the collapse of the edifice. Other factors that could have contributed to this collapse of the volcano are (Keating and McGuire 2000):

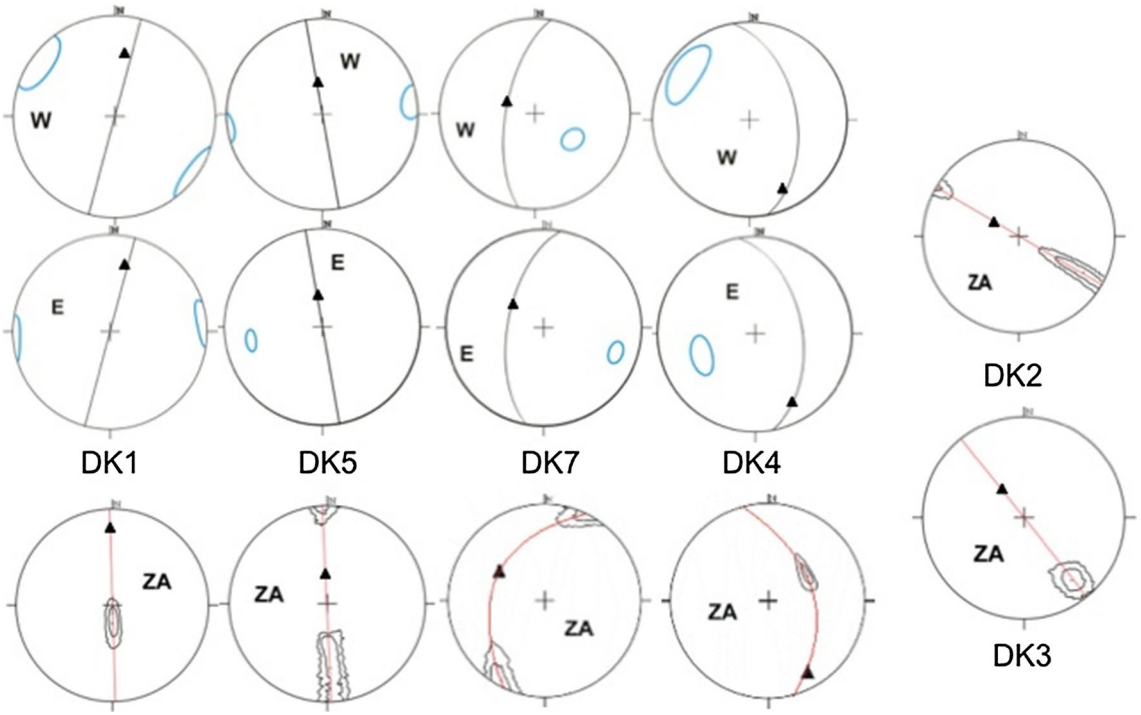

Fig. 11 Above: from dikes yielding reliable data (after rejection of abnormal fabric; see text), minimum confidence zone at 95% (Henry and Le Goff 1995). For K_{min} axes(the great circle represents orientation of the dike plane, from field measurements). Below: magnetic zone axis (MZA), except for DK6 where it cannot be determined (too few normal fabrics), with its confidence zones at 95% and 63% (Henry 1997). Inferred flow direction is indicated by triangles (Schmidt diagrams, lower hemisphere). The orientation of the dike plane, suggested as materialized by the plane including the lengthening of the MZA confidence zone (red line), is slightly different from that obtained by the field measurement. The later is often only a rough estimate, particularly for the Hawaiian dikes, and the data from the MZA probably allow a more precise determination of this plane

rapid accumulation of lavas, high angle of repose of the flanks of the volcano causing a lack of stability in the pile of lavas, unstable foundation, thermal alteration, edifice pore pressure, un-buttressed structure; and buried faults.

Our results are in contrast with lateral magma flows, deduced from the AMS study of dikes in other highly dissected volcanic edifices, such as the Koolau volcano (Knight and Walker 1988; Herrero-Bervera et al. 2002a, b; Walker 1986, 1987, 1990; Walker et al. 1995) and the volcanic system of the Isle of Skye, Scotland (Herrero-Bervera et al. 2001).

A better evaluation of the flank collapses of the Wai'anae edifice requires further studies, especially of AARM, but also of more AMS investigations dikes from the north, east, and west parts of the caldera (Fig. 1).

Additional file

Additional file 1. Hysteresis plots of seven pilot dikes from the Wai'anae volcano, Oahu, Hawaii. Notice the low-coercivity (e.g., Dikes 1,6 and 7) versus high-coercivity results of dikes (e.g., Dikes 4 and 5).

Abbreviations

AMS: anisotropy of magnetic susceptibility; D: declination; DC: direct current; DK: dike; E: East; GAP: gradient acquisition plot; HIGP: Hawaii Institute of Geophysics and Planetology; I: inclination; IRM: isothermal remanent magnetization; K_{max}: maximum principal susceptibility; K_{int}: intermediate principal susceptibility; K_{min}: minimum principal susceptibility; $K(T)$: low-field susceptibility versus temperature; LAP: linear acquisition plot; mT: milli-Tesla; Mr: magnetization remanence; Ms: magnetization saturation; MZA: magnetic zone axis; NNW–SSE: northnorthwest–southsoutheast; NW–SE: northwest–southeast; NNW–SSE: northnorthwest–southsoutheast; NW–W: northwest–west; NW–ESE: northwest–eastsoutheast; PSD: pseudo-single domain; P': corrected anisotropy degree; SD: single domain; SIRM: saturation isothermal remanent magnetization; SOEST: School of Ocean Earth Science and Technology; T: shape parameter; VFTB: variable field translation balance; W: west.

Authors' contributions

The authors contributed to the methodology, data processing and interpretation of this manuscript. The manuscript was improved with helpful contributions from co-authors. All authors read and approved the final manuscript.

Author details

[1] Petrofabrics and Paleomagnetics Laboratory, SOEST-Hawaii Institute of Geophysics and Planetology, University of Hawaii at Manoa, 1680 East-West Road, POST 602, Honolulu, HI 96822, USA. [2] Paléomagnétisme, Institut de Physique du Globe de Paris, Sorbonne Paris Cité, Univ. Paris Diderot and UMR 7154 CNRS, 4 avenue de Neptune, 94107 Saint-Maur Cedex, France. [3] Instituto Dom Luís, Faculdade de Ciências da Universidade de Lisboa, Lisbon, Portugal. [4] Área Departamental de Física, Instituto Superior de Engenharia de Lisboa, 1 Rua Conselheiro Emídio Navarro, 1959-007 Lisbon, Portugal.

Acknowledgements
We gratefully acknowledge the assistance of James Lau during the fieldwork and laboratory phases of the project. This is SOEST Contributions #10317 and HIGP # 2280. We acknowledge the assistance of the EPS Editor, Associate Editor, and the time and effort of the reviewers for their very useful and constructive comments to greatly improve the manuscript and make it publishable.

Competing interests
The authors declare that they have no competing interests.

Availability of data and materials
The data are available in Table 1 and also the magnetic grain size data as a table in supplement.

Funding
Funding for this research was provided to Emilio Herrero-Bervera by HIGP-SOEST of the University of Hawaii at Manoa. This is SOEST Contributions #10317 and HIGP # 2280. Funding for Bernard Henry was provided by IPGP, Paris France. Funding for Mario Moreira was provided by Instituto Dom Luís, FCT/UID/GEO/50019.

Publisher's Note

Received: 5 May 2018 Accepted: 21 November 2018
Published online: 06 December 2018

References

Aifa T, Lefort JP, Guennoc P (1999) Anisotropy of magnetic susceptibility investigations of the St Malo dyke swarm (Brittany, France): emplacement mechanism of doleritic intrusions. Geophys J Int 139:573–582

Archanjo CJ, Araújo MGS, Launeau P (2002) Fabric of the Rio Ceará–Mirin mafic dike swarm (northeastern Brazil) determined by anisotropy of magnetic susceptibility and image analysis. J Geophys Res 107:B3. https://doi.org/10.1029/2001JB000268

Aubourg C, Tshoso G, Le Gall B, Bertrand H, Tiercelin JJ, Kampunzu AB, Dyment J, Modisi M (2008) Magma flow revealed by magnetic fabric in the Okavango giant dyke swarm, Karoo igneous province, northern Botswana. J Volcanol Geotherm Res 170:247–261

Battaglia M, Di Baria M, Acocella V, Neri M (2011) Dike emplacement and flank instability at Mount Etna: constraints from a poro-elastic model of flank collapse. J Volcanol Geotherm Res 199:153–164

Callot JP, Geoffroy L (2004) Magma flow in the East Greenland dyke swarm inferred from study of anisotropy of magnetic susceptibility: magmatic growth of a volcanic margin. Geophys J Int 159:816–830. https://doi.org/10.1111/j.1365-246X.2004.02426.x

Callot JP, Guichet X (2003) Rock texture and magnetic lineation in dykes: a simple analytical model. Tectonophysics 366:207–222

Callot JP, Geoffroy L, Aubourg C, Pozzi JP, Mege D (2001) Magma flow directions of shallow dykes from the East Greenland volcanic margin inferred from magnetic fabric studies. Tectonophysics 335:313–329

Cañón Tapia E, Chávez Álvarez MJ (2004) Rotation of uni-axial ellipsoidal particles during simple shear revisited: the influence of elongation ratio, initial distribution of a multiparticle system and amount of shear in the acquisition of a stable orientation. J Struct Geol 26:2073–2087

Cañón-Tapia E (1996) Single-grain versus distribution anisotropy: a simple three-dimensional model. Phys Earth Planet Inter 94:149–158

Cañón-Tapia E (2004) Anisotropy of magnetic susceptibility of lava flows and dykes: a historical account. Geol Soc Lond Spec Publ 238:205–225

Cañón-Tapia E, Herrero-Bervera E (2009) Sampling strategies and the anisotropy of magnetic susceptibility of dykes. Tectonophysics 466:3–17

Cañón-Tapia E, Walker GPL, Herrero-Bervera E (1995) Magnetic fabric and flow direction in basaltic Pahoehoe lava of Xitle Volcano, Mexico. J Volcanol Geotherm Res 65:249–263

Cañón-Tapia E, Walker GPL, Herrero-Bervera E (1996) The internal structure of lava flows-insights from AMS measurements I: near Vent a'a. J Volcanol Geotherm Res 70:21–36

Chadima M, Cajz V, Týcová P (2009) On the interpretation of normal and inverse magnetic fabric in dikes: examples from the Eger Graben, NW Bohemian Massif. Tectonophysics 466:47–63. https://doi.org/10.1016/j.tecto.2008.09.005

Coombs ML, Clague DAF, Moore FB, Cousens L (2004) Growth and collapse of Waianae Volcano, Hawaii, as revealed by exploration of its submarine flanks. Geochem Geophys Geosyst 5:Q08006. https://doi.org/10.1029/2004GC000717

Costa ACG, Hildenbrand A, Marques FO, Sibrant ALR, Santos de Campos A (2015) Catastrophic flank collapses and slumping in Pico Island during the last 130 kyr (Pico-Faial ridge, Azores Triple Junction). J Volcanol Geotherm Res 302:33–46

Day R, Fuller M, Schmidt VA (1977) Hysteresis properties of titanomagnetites: grain size and compositional dependence. Phys Earth Planet Inter 13:260–267

Day SJ, Heleno da Silva SIN, Fonseca JFBD (1999) A past giant lateral collapse and present-day flank instability of Fogo, Cape Verde Islands. J Volcanol Geotherm Res 94(1–4):191–218. https://doi.org/10.1016/S0377-0273(99)00103-1

Delcamp A, Petronis MS, Troll VR (2014) Discerning magmatic flow patterns in shallow-level basaltic dykes from the NE rift zone of Tenerife, Spain, using the Anisotropy of Magnetic Susceptibility (AMS) technique. Geol Soc London Spec Publ 396:87–105. https://doi.org/10.1144/SP396.2

Doell RR, Dalrymple B (1973) Potassium-argon ages and paleomagnetism of the Waianae and Koolau volcanic series, Oahu, Hawaii. Geol Soc Am Bull 84:1217–1242

Dragoni M, Lanza R, Tallarico A (1997) Magnetic anisotropy produced by magma flow: theoretical model and experimental data from Ferrar dolerite sills (Antarctica). Geophys J Int 128:230–240

Dunlop DJ (2002) Theory and application of the Day plot (Mrs/Ms versus Hcr/Hc). 1. Theoretical curves and tests using titanomagnetite data. J Geophys Res 107:(B3)

Dunlop DJ, Özdemir Ö (1997) Rock magnetism: fundamentals and frontiers. Cambridge Univeristy Press, Cambridge

Ellwood BB (1978) Flow and emplacement direction determined for selected basaltic bodies using magnetic susceptibility anisotropy measurements. Earth Planet Sci Lett 41:254–264

Elsworth D, Day SJ (1999) Flank collapse triggered by intrusion: the Canarian and Cape Verde Archipelagoes. J Volcanol Geotherm Res 94:323–340

Fanjat G, Camps P, Shcherbakov V, Barou F, Sougrati MT, Perrin M (2012) Magnetic interactions at the origin of abnormal magnetic fabrics in lava flows: a case study from Kerguelen flood basalts. Geophys J Int 189(2):815–832

Féménias O, Diot H, Berza T, Gauffriau A, Demaiffe D (2004) Asymmetrical to symmetrical magnetic fabric of dikes: Paleo-flow orientation and Paleo-stresses recorded on feeder-bodies from the Motru Dike Swarm (Romania). J Struct Geol 26:1401–1418

Ferré EC (2002) Theoretical models of intermediate and inverse AMS fabrics. Geophys Res Lett. https://doi.org/10.1029/2001GL014367

Fisher RA (1953) Dispersion on a sphere. Proc R Soc Lond A 17:295–305

Geoffroy L, Callot JP, Aubourg C, Moreira M (2002) Magnetic and plagioclase linear fabric discrepancy in dykes: a new way to define the flow vector using magnetic foliation. Terra Nova 14:183–190

Grégoire V, Darrozes J, Gaillot P, Nédélec A (1998) Magnetite grain shape fabric and distribution anisotropy vs. rock magnetic fabric: a three-dimensional case study. J Struct Geol 20:937–944

Hargraves RB, Johnson D, Chart CY (1991) Distribution anisotropy: the cause of AMS in igneous rocks? Geophys Res Lett 18:2193–2196

Henry B (1974) Sur l'anisotropie de susceptibilité magnétique du granite récent de Novate (Italie du Nord). C R Acad Sci Paris 278(C):1171–1174

Henry B (1997) The magnetic zone axis: a new element of magnetic fabric for the interpretation of the magnetic lineation. Tectonophysics 271:325–329

Henry B (2007) Changes in magnetic mineralogy due to heating and methodological implications. In: Gubbins D, Herrero-Bervera E (eds) Encyclopedia of geomagnetism and paleomagnentism. Springer, Netherlands, pp 512–515

Henry B, Le Goff M (1995) Application de l'extension bivariate de la statistique de Fisher aux données d'anisotropie de susceptibilité magnétique: intégration des incertitudes de mesure sur l'orientation des directions principales. C R Acad Sci Paris 320(11):1037–1042

Henry B, Camps P, Plenier G (2003) Magnetic fabric of Miocene lavas in the Jeanne d'Arc peninsula (Kerguelen islands). J Volcanol Geotherm Res 127:153–164
Herrero-Bervera E, Coe RS (1999) Transitional behavior during the Gilbert–Gauss and Lower Mammoth reversals recorded in lavas from the Wai'anae volcano, O'ahu, Hawaii. J Geophys Res 104:29157–29173
Herrero-Bervera E, Valet JP (1999) Paleosecular variation during sequential geomagnetic reversals from Hawaii. Earth Planet Sci Lett 171:139–148
Herrero-Bervera E, Valet JP (2005) Absolute paleointensity and reversal records from the Waianae sequence (Oahu, Hawaii, USA). Earth Planet Sci Lett 234:279–296. https://doi.org/10.1016/j.epsl.2005.02.032
Herrero-Bervera E, Valet JP (2009) Testing determinations of absolute paleointensity from the 1955 and 1960 Hawaiian flows. Earth Planet Sci Lett 287:420–433. https://doi.org/10.1016/j/epsl.2009.08.035
Herrero-Bervera E, Walker GPL, Canon-Tapia E, Garcia MO (2001) Magnetic fabric and inferred flow direction of dikes, conesheets and sill swarms, Isle of Skye, Scotland. J Volcanol Geotherm Res 106:195–210
Herrero-Bervera E, Canon-Tapia E, Walker GPL, Tanaka H (2002a) Magnetic fabric study and inferred flow directions of lavas of the Old Pali Road, O'ahu, Hawai'i. J Volcanol Geotherm Res 118:161–171
Herrero-Bervera E, Canon-Tapia E, Walker GPL, Guerrero-Garcia JC (2002b) The Nuuanu and Wailau giant landslides: insights from paleomagnetic and anisotropy of magnetic susceptibility (AMS) studies. Phys Earth Planet Inter 129:83–98
Hext G (1963) The estimation of second-order tensors, with related tests and designs. Biometrika 50:353
Hildenbrand A, Gillot PY, Bonneville A (2006) Offshore evidence for a huge landslide of the northern flank of Tahiti-Nui (French Polynesia). Geochem Geophys Geosyst 7(3):Q03006. https://doi.org/10.1029/2005GC001003
Hrouda F, Ježek J (2017) Role of single-domain magnetic particles in creation of inverse magnetic fabrics in volcanic rocks: a mathematical model study. Stud Geophys Geod 61:145–161. https://doi.org/10.1007/s11200-015-0675-6
Hrouda F, Burianek D, Krejci O, Chadima M (2015) Magnetic fabric and petrology of Miocene sub-volcanic sills and dikes emplaced into the SW Flysch Belt of the West Carpathians (S Moravia, Czech Republic) and their volcanological and tectonic implications. J Volcanol Geotherm Res 290:23–38. https://doi.org/10.1016/j.jvolgeores.2014.12.001
Jelinek V (1978) Statistical processing of magnetic susceptibility measured in groups of specimens. Stud Geophys Geod 22:50–62
Jelinek V (1981) Characterization of the magnetic fabric of rocks. Tectonophysics 79:63–67
Jordanova D, Jordanova N (2016) Thermomagnetic behavior of magnetic susceptibility, heating rate and sample size effects. Front Earth Sci 3:90. https://doi.org/10.3389/feart.2015.00090
Keating BH, McGuire WJ (2000) Island edifice failures and associated Tsunami hazards. Pure Appl Geophys 157:899–955
Khan MA (1962) The anisotropy of magnetic susceptibility of some igneous and metamorphic rocks. J Geophys Res 67(7):2874–2885
Knight MD, Walker GPL (1988) Magma flow directions in dikes of the Koolau Complex, Oahu, determined from magnetic fabric studies. J Geophys Res 93(B5):4301–4319
Krasa D, Herrero-Bervera E (2005) Alteration induced changes of magnetic fabric as exemplified by dykes of the Koolau volcanic range. Earth Planet Sci Lett 240:445–453
Kruiver P, Dekkers M, Heslop D (2001) Quantification of magnetic coercivity components by the analysis of acquisition curves of isothermal remanent magnetisation. Earth Planet Sci Lett 189:269–276
Leiss B et al (2000) Recent developments and goals in texture research of geological materials. J Struct Geol 22:1531–1540
Lipman PW, Normark WR, Moore JG, Wilson JB, Gutmacher CE (1988) The giant submarine Alika debris slide, Mauna Loa, Hawaii. J Geophys Res 93(B5):4279–4299. https://doi.org/10.1029/JB093iB05p04279
McDonald GA (1940) Petrography of the Waianae range, Oahu. Terr Hawaii Div Hydrogr Bull 5:63–91
Moore JG., Clague DA (2002) Mapping the Nuuanu and Wailau landslides in Hawaii. In: Takahashi E, Lipman PW, Garcia MO, Naka J, Aramaki S (eds) Hawaiian volcanoes: deep underwater perspectives. American Geophysical Monograph Series, vol 128. American Geophysical Union, Washington, pp 223–244. http://dx.doi.org/10.1029/GM128
Moore JG, Clague DA, Holcomb RT, Lipman PW, Normark WR, Torresan ME (1989) Prodigious submarine landslides on the Hawaiian Ridge. J Geophys Res 94(B12):17465–17484. https://doi.org/10.1029/JB094iB12p17465
Moreira M, Geoffroy L, Pozzi JP (1999) Ecoulement magmatique dans les dykes du point chaud des Açores: étude préliminaire par anisotropie de susceptibilité magnétique (ASM) dans l'île de San Jorge. C R Acad Sci Paris IIA 329:15–22. https://doi.org/10.1016/S1251-8050(99)80222-5
Moreira M, Geoffroy L, Pozzi JP (2014) Magma flow pattern in dikes of the Azores revealed by anisotropy of magnetic susceptibility. J Geophys Res. https://doi.org/10.1002/2014JB010982
Park JK, Tanczyk EI, Desbarats A (1988) Magnetic fabric and its significance in the 1400 Ma Mealy diabase dykes of Labrador, Canada. J Geophys Res 93:13689–13704
Petrovský E, Kapička A (2006) On determination of the Curie point from thermomagnetic curves. J Geophys Res 111(B12):B12S27/1-10. ISSN 0148-0227
Potter DK, Stephenson A (1988) Single-domain particles in rocks and magnetic fabric analysis. Geophys Res Lett 15:1097–1100
Presley T, Sinton J, Pringle N (1998) Post-shield volcanism and catastrophic mass wasting of the Waianae Volcano, Oahu, Hawaii. Bull Volcanol 58:597–616
Raposo MIB (1997) Magnetic fabric and its significance in the Florianópolis dyke swarm, southern Brazil. Geophys J Int 131:159–170
Raposo MIB (2011) Magnetic fabric of the Brazilian dike swarms: a review. In: Petrovsky E et al (eds) The Earth's magnetic interior, IAGA Special Sopron Book Series 1, Springer, Berlin, https://doi.org/10.1007/978-94-007-0323-0_17
Raposo MIB, Ernesto M (1995) Anisotropy of magnetic susceptibility in the Ponta Grossa dyke swarm (Brazil) and its relationship with magma flow direction. Phys Earth Planet Inter 87:183–196
Reid ME, Sisson TW, Brien DL (2001) Volcano collapse promoted by hydrothermal alteration and edifice shape, Mount Rainier, Washington. Geology 29:779–782
Robertson DJ, France DE (1994) Discrimination of remanence-carrying minerals in mixtures, using isothermal remanent magnetisation acquisition curves. Phys Earth Planet Inter 82:223–234
Rochette P (1988) Inverse magnetic fabric in carbonate-bearing rocks. Earth Planet Sci Lett 90:229–237
Rochette P, Jenatton L, Dupuy C, Boudier F, Reuber L (1991) Diabase dikes emplacement in the Oman ophiolite: a magnetic fabric study with reference to geochemistry. In: Peters T (ed) Ophiolite genesis and evolution of the oceanic lithosphere. Ministry of Petroleum Mineral, Muscat, pp 55–82
Rochette P, Aubourg C, Perrin M (1999) Is this magnetic fabric normal? A review and case studies in volcanic formations. Tectonophysics 307:219–234
Rubin AM, Pollard DD (1988) Origins of blade-like dikes in volcanic rifts zones. In: Decker RW, Wright TL, Sauffer PH (eds) Volcanism in Hawaii, U.S. Geological Survey Professional Paper 1350, USGS, Reston, pp 1449–1470
Schöbel S, de Wall H (2014) AMS-NRM interferences in the Deccan basalts: Toward an improved understanding of magnetic fabrics in flood basalts. J Geophys Res 119:2651–2678. https://doi.org/10.1002/2013JB10660
Silva PF, Marques FO, Henry B, Mateus A, Lourenço N, Miranda JM (2004) Preliminary results of a study of magnetic properties in the Foum-Zguid dyke (Morocco). Phys Chem Earth 29:909–920
Silva PF, Marques FO, Henry B, Mateus A, Vegas R, Miranda JM, Palomino R, Palencia-Ortas A (2008) Magma flow, exsolution processes and rock metasomatism in the Great Messejana–Plasencia dyke (Iberian Peninsula). Geophys J Int 175:806–824. https://doi.org/10.1111/j.1365-246X.2008.03920.x
Silva PF, Marques FO, Henry B, Madureira P, Hirt AM, Font E, Lourenço N (2010) Thick dyke emplacement and internal flow: a structural and magnetic fabric study of the deep-seated dolerite dyke of Foum Zguid (southern Morocco). J Geophys Res 115:B12108. https://doi.org/10.1029/2010JB007638
Silva PF, Henry B, Marques FO, Hildenbrand A, Madureira P, Mériaux C, Kratinová Z (2012) Palaeomagnetic study of a sub-aerial volcanic ridge (São Jorge Island, Azores) for the past 1.3 Myr: evidence for the Cobb Mountain Subchron, volcano flank instability and tectono-magmatic implications. Geophys J Int 188:959–978
Silva PF, Marques FO, Hirt AM, Machek M, Kratinova Z, Henry B, Madureira P (2014) Evidence for non-coaxiality between ferromagnetic and

paramagnetic fabrics developed during magma flow and cooling of a thick mafic dyke. Tectonophysics 629:155–164. https://doi.org/10.1016/j.tecto.2014.04.017
Silva PF, Henry B, Marques FO, Hildenbrand A, Lopes A, Madureira P, Madeira J, Nunes JC, Roxerova Z (2018) Volcano-tectonic framework of a linear volcanic ridge (Faial-Pico ridge, Azores Archipelago) assessed by paleomagnetic studies. J Volcanol Geotherm Res 352:78–91
Sinton J (1979) Geology and petrography of volcanic rocks of Lualualei Valley. Waianae Range, Oahu. In: Garcia MO, Sinton JM (eds) Field trip guide to the Hawaiian Islands, HIG Special Publications. Hawaii Institute of Geophysics, Honolulu, pp 51–66
Sinton J (1986) Revision of stratigraphic nomenclature of Wai'anae volcano, O'ahu, Hawai'i. US Geol Surv Bull 1775-A:A9–A15
Soriano C, Beamud E, Garces M, Ort MH (2016) "Anomalous" magnetic fabrics of dikes in the stable single domain/superparamagnetic threshold. Geophys J Int 204:1040–1059
Stacey FD (1960) Magnetic anisotropy of igneous rocks. J Geophys Res 65:2429–2442
Staudigel H, Gee J, Tauxe L, Varga RJ (1992) Shallow intrusive directions of sheeted dikes in the Troodos ophiolite: anisotropy of magnetic susceptibility and structural data. Geology 20:841–844
Stearns HT (1940) Geologic map and guide of the island of Oahu, Hawaii. Div Hydrogr Bull 2:1–75
Tauxe L, Gee JS, Staudigel H (1998) Flow directions in dikes from anisotropy of magnetic susceptibility data: the bootstrap way. J Geophys Res 103(B8):17775–17790
Trusdell FA (2012) Mauna-Loa-History, hazards, and risk of living with the world's largest volcano, U.S. Geological Survey Fact Sheet, 2012-3104. https://pubs.usgs.gov/fs/2012/3104/
Voight B, Elsworth D (1997) Failure of volcano slopes. Géotechnique 47:1–31
Walker GPL (1986) Koolau dike complex, Oahu intensity and origin of a sheeted dike complex high in a Hawaiian volcanic edifice. Geology 14:310–313
Walker GPL (1987) The dyke complex of Koolau volcano, Oahu: internal structure of a Hawaiian rift zone. In: Decker RW, Wright TL, Stauffer PH (eds) Hawaiian volcanism, U.S. Government Printing Office, Washington, U.S. Geological Survey Professional Paper 1350, pp 961–993
Walker GPL (1990) Geology and volcanology of the Hawaiian Islands. Pac Sci 44:315–347
Walker GPL, Eyre P, Spengler R, Knight MD, Kennedy K (1995) Congruent dyke-widths in large basaltic volcanoes. In: Baer G, Heimann A (eds) Physics and chemistry of dykes. Balkema, Rotterdam, pp 35–40
Yang X, Davis PM (1992) Geodetic analysis of dike intrusion and motion of the magma reservoir beneath the summit of Kilauea volcano, Hawaii: 1970—1985. J Geophys Res 97:3305–3324
Yokose H (2002) Landslides on the windward flanks of Oahu and Molokai, Hawaii: SHINKAI 6500 submersible investigations. In: Hawaiian volcanoes, American Geophysics Union Monograph 128, pp 245–262
Zbinden EA, Sinton JM (1988) Dikes and the petrology of Waianae Volcano, Oahu. J Geophys Res 93:14856–14866